Probing gravitational wave polarizations with signals from compact binary coalescences

Maximiliano Isi[1,*] and Alan J. Weinstein[1]

[1] *LIGO Laboratory, California Institute of Technology, Pasadena, California 91125, USA*

(Dated: October 6, 2017)

In this technical note, we study the possibility of using networks of ground-based detectors to directly measure gravitational-wave polarizations using signals from compact binary coalescences. We present a simple data analysis method to partially achieve this, assuming presence of a strong signal well-captured by a GR template.

I. INTRODUCTION

The detection of gravitational waves (GWs) by the Advanced Laser Interferometer Gravitational-Wave Observatory (aLIGO) has enabled some of the first experimental studies of gravity in the highly dynamical and strong-field regimes [1–5]. These first few detections have already been used to place some of the most stringent constraints on deviations from the general theory of relativity (GR) in this domain, which is inaccessible to laboratory, Solar System or cosmological tests of gravity.

However, it has not been possible to use LIGO signals to learn about the polarization content of GWs [5], a measurement highly relevant when comparing GR to many of its alternatives [6, 7]. In fact, all existing observations are so far consistent with the extreme case of purely non-GR polarizations. The reason for this is that the two LIGO instruments are nearly coaligned, meaning that they are sensitive to approximately the same linear combination of polarizations. This makes it nearly impossible to unequivocally characterize the polarization content of transient GW signals like the compact-binary coalescences (CBCs) observed so far, at least not without making assumptions about the way the signals were sourced [7, 8].

Existing observations that are usually taken to constrain the amount of allowed non-GR polarizations can do so only in an indirect manner. For example, measurements of the orbital decay of binary systems are sensitive to the total radiated GW power, but do not probe the geometric effect (namely, the directions in which space is stretched and squeezed) of the waves directly (see e.g. [9, 10], or [11, 12] for reviews). In the context of specific alternative theories (e.g. scalar-tensor) such observations can indeed constrain the power contained in extra polarizations. However, such measurements provide no direct, model-independent information on the actual polarization content of the gravitational radiation. Thus, there may be multiple theories, with different polarization content, that still predict the correct observed GW emitted power.

To see that the above is the case, consider a scenario in which GWs are emitted precisely as in GR, but where the polarizations change during propagation: the phase evolution would be similar to GR, but the geometric effect of the wave would be completely different [13–16]. (This polarization mutation could take place if the linear polarization basis does not diagonalize the kinetic matrix of the theory, as is the case for neutrino oscillations [17, 18], or for the circular GW polarization states in dynamical Chern-Simons gravity [19].) Because the same limitations of pulsar binary analyses apply to studies of the details in the phasing of signals previously detected with LIGO, and other traditional tests of GR (like Solar System tests) have no bearing on GWs, there currently exist no direct measurements of GW polarizations.

Prospects for the direct measurement of GW polarizations are improved by the addition of Advanced Virgo to the detector network. In principle, at least five non-coaligned differential-arm detectors would be needed to break *all* the degeneracies among the five nondegenerate polarizations allowed by generic metric theories of gravity [20, 21], if transient signals are used [22, 23]. However, as we will show, the current Advanced-LIGO–Advanced-Virgo network can already be used to distinguish between *some* of the possible combinations of polarizations without the need to use specific knowledge about the phase evolution of the source.

In this note, we present a simple Bayesian method to extract information about GW polarizations directly from strong CBC signals by using the relative amplitudes and timing at the different detectors.

II. BACKGROUND

A. Polarizations

In all theories that respect Einstein's equivalence principle, including GR, gravitational interactions may be fully described via the universal coupling of matter to a metric tensor [6, 24]. Because of this, it may be shown that, in any such *metric theory*, a (nearly-)null plane GW may be encoded in at most six independent components of the Riemann tensor at any given point in spacetime [6, 20, 21]. These degrees of freedom give rise to six geometrically distinct polarizations, corresponding to the six linearly independent components of an arbitrary metric perturbation.

At any given spacetime point $\vec{x}$, the metric perturbation

* misi@ligo.caltech.edu

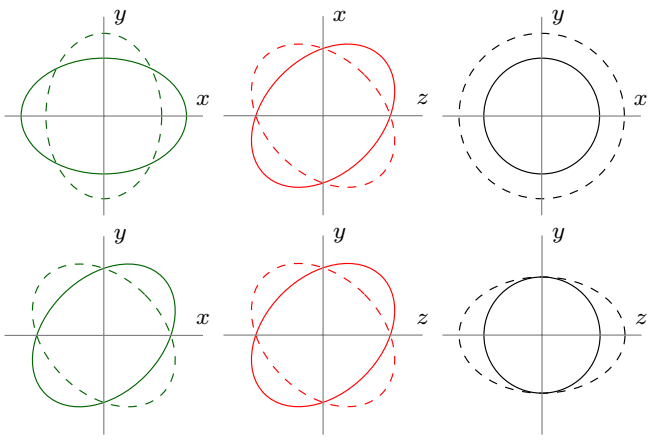

FIG. 1. *Effect of different GW polarizations on a ring of free-falling test particles.* Plus (+) and cross (×) tensor modes (green); vector-x (x) and vector-y (y) modes (red); breathing (b) and longitudinal (l) scalar modes (black). In all of these diagrams the wave propagates in the z direction. This decomposition into polarizations was first proposed for generic metric theories in [21].

may thus be written as

$$h_{ab}(\vec{x}) = h_A(\vec{x})\, e^A_{\ ab}\,, \tag{1}$$

for six independent amplitudes, $h_A(\vec{x})$, and six polarization tensors $e^A_{\ ab}$ (implicit sum over polarizations A). For instance, letting $\mathbf{w}_z = \mathbf{w}_x \times \mathbf{w}_y$ be a spatial unit vector in the direction of propagation of the wave, we may consider the set of linear polarization tensors

$$\mathbf{e}^{+} = \mathbf{w}_x \otimes \mathbf{w}_x - \mathbf{w}_y \otimes \mathbf{w}_y\,, \tag{2}$$

$$\mathbf{e}^{\times} = \mathbf{w}_x \otimes \mathbf{w}_y + \mathbf{w}_y \otimes \mathbf{w}_x\,, \tag{3}$$

$$\mathbf{e}^{\mathrm{x}} = \mathbf{w}_x \otimes \mathbf{w}_z + \mathbf{w}_z \otimes \mathbf{w}_x\,, \tag{4}$$

$$\mathbf{e}^{\mathrm{y}} = \mathbf{w}_y \otimes \mathbf{w}_z + \mathbf{w}_z \otimes \mathbf{w}_y\,, \tag{5}$$

$$\mathbf{e}^{\mathrm{b}} = \mathbf{w}_x \otimes \mathbf{w}_x + \mathbf{w}_y \otimes \mathbf{w}_y\,, \tag{6}$$

$$\mathbf{e}^{\mathrm{l}} = \mathbf{w}_z \otimes \mathbf{w}_z\,. \tag{7}$$

Then Eq. (1) implies that there exists some gauge in which, in a local Lorentz frame with Cartesian coordinates along $(\mathbf{w}_x, \mathbf{w}_y, \mathbf{w}_z)$,

$$[h_{ij}] = \begin{pmatrix} h_{\mathrm{b}} + h_{+} & h_{\times} & h_{\mathrm{x}} \\ h_{\times} & h_{\mathrm{b}} - h_{+} & h_{\mathrm{y}} \\ h_{\mathrm{x}} & h_{\mathrm{y}} & h_{\mathrm{l}} \end{pmatrix}, \tag{8}$$

where the h_A's represent the amplitudes of the linear polarizations: plus (+), cross (×), vector x (x), vector y (y), breathing (b) and longitudinal (l). The effect of each of these modes on a ring of freely-falling particles is represented in Fig. 1.

Polarizations may be characterized by their behavior under Lorentz transformations, and different theories may be classified according to the polarizations they allow, as seen by different observers; this is known as the E(2) or *Eardley* classification [20, 21]. From a field-theoretic perspective, the two tensor modes, the two vector modes and the breathing (transverse) scalar mode correspond to the helicity ±2, helicity ±1, and helicity 0 states of a massive spin-2 particle (the graviton). The remaining longitudinal scalar mode is usually linked to a ghost-like degree of freedom (associated with the trace). This correspondence between geometric (Eardly's classification) and field-theoretic (Wigner's classification) language is, however, limited because the the E(2) classification is only semi-Lorentz-invariant (although it is usually taken to hold, at least in the weak field regime) [21].

Einstein's theory only allows for the existence of linear combinations of the tensor + and × polarizations [6]. On the other hand, scalar-tensor theories famously predict the presence of some breathing component associated with the theory's extra scalar field [25], as do some theories with extra dimensions [26]. On top of tensor and scalar modes, bimetric theories, like Rosen or Lightman-Lee theories, may also predict vector modes [8, 27, 28]. The same is true in general for massive-graviton frameworks [29]. Furthermore, less conventional theories might, in principle, predict the existence of vector or scalar modes *only*, while still possibly being in agreement with all other non-GW tests of GR (see e.g. [30], for an unconventional example).

B. Antenna patterns

Because different polarizations have geometrically distinct effects, as illustrated in Fig. 1, GW detectors will react differently to each mode. The *strain* produced by a GW metric perturbation h_{ab} on certain detector I spatially located at $\mathbf{x}_I$, is given by

$$h_I(t) = D^{ab}_I h_{ab}(t, \mathbf{x}_I) = h_A(t, \mathbf{x}_I) D^{ab}_I e^A_{ab}. \tag{9}$$

The detector tensor, D^{ab}, encodes the geometry of the instrument and the measurement it makes; for diferential-arm detectors (sometimes called *quadrupolar antennas*, because of the symetries of their angular response functions, cf. Fig. 2), like LIGO and Virgo, this is

$$D^{ab} = \frac{1}{2}\left(d_x{}^a d_x{}^b - d_y{}^a d_y{}^b\right), \tag{10}$$

where $\mathbf{d}_x$ and $\mathbf{d}_y$ are spatial unit vectors along the detector arms (with common origin at the vertex $\mathbf{x}_I$). Although D^{ab} is technically also a function of time due to the motion of Earth with respect to the fixed stars, in practice it can be taken as constant when treating short-lived CBC signals, as is done here.

The $h_A(t)$'s are determined by a nontrivial combination of the source dynamics, the details of the matter-gravity coupling, and the vacuum structure of the theory. However, the response (*antenna pattern*) of detector I to polarization A,

$$F^A \equiv D_I^{ab} e_{ab}^A \,, \tag{11}$$

depends *only* on the local geometry of the gravitational wave and the detector, irrespective of the properties of the source. This decoupling makes the antenna patterns a unique resource for studying GW polarizations directly.

The response functions, Eq. (11), encode the effect of a linearly A-polarized GW with unit amplitude, $h_A = 1$. Ground-based GW detectors, like LIGO and Virgo are quadrupolar antennas that perform low-noise measurements of the strain associated with the differential motion of two orthogonal arms. Their detector response functions can thus be written as [31–34]:

$$F_+ = \frac{1}{2}\left[(\mathbf{w}_x\cdot\mathbf{d}_x)^2 - (\mathbf{w}_x\cdot\mathbf{d}_y)^2 - (\mathbf{w}_y\cdot\mathbf{d}_x)^2 + (\mathbf{w}_y\cdot\mathbf{d}_y)^2\right], \tag{12}$$

$$F_\times = (\mathbf{w}_x\cdot\mathbf{d}_x)(\mathbf{w}_y\cdot\mathbf{d}_x) - (\mathbf{w}_x\cdot\mathbf{d}_y)(\mathbf{w}_y\cdot\mathbf{d}_y), \tag{13}$$

$$F_{\rm x} = (\mathbf{w}_x\cdot\mathbf{d}_x)(\mathbf{w}_z\cdot\mathbf{d}_x) - (\mathbf{w}_x\cdot\mathbf{d}_y)(\mathbf{w}_z\cdot\mathbf{d}_y), \tag{14}$$

$$F_{\rm y} = (\mathbf{w}_y\cdot\mathbf{d}_x)(\mathbf{w}_z\cdot\mathbf{d}_x) - (\mathbf{w}_y\cdot\mathbf{d}_y)(\mathbf{w}_z\cdot\mathbf{d}_y), \tag{15}$$

$$F_{\rm b} = \frac{1}{2}\left[(\mathbf{w}_x\cdot\mathbf{d}_x)^2 - (\mathbf{w}_x\cdot\mathbf{d}_y)^2 + (\mathbf{w}_y\cdot\mathbf{d}_x)^2 - (\mathbf{w}_y\cdot\mathbf{d}_y)^2\right], \tag{16}$$

$$F_{\rm l} = \frac{1}{2}\left[(\mathbf{w}_z\cdot\mathbf{d}_x)^2 - (\mathbf{w}_z\cdot\mathbf{d}_y)^2\right]. \tag{17}$$

Here, as before, the spatial vectors $\mathbf{d}_x$, $\mathbf{d}_y$ have unit norm and point along the detector arms such that $\mathbf{d}_z = \mathbf{d}_x \times \mathbf{d}_y$ is the local zenith; the direction of propagation of the wave from a source at known sky location (specified by right ascension α, and declination δ) is given by $\mathbf{w}_z$, and $\mathbf{w}_x$, $\mathbf{w}_y$ are such that $\mathbf{w}_z = \mathbf{w}_x \times \mathbf{w}_y$. We choose $\mathbf{w}_x$ to lie along the intersection of the equatorial plane of the source with the plane of the sky, and let the angle between $\mathbf{w}_y$ and the celestial north be ψ, the *polarization angle*.

Because of their symmetries, the breathing and longitudinal modes are fully degenerate to networks of quadrupolar antennas (see e.g. Sec. VI of [8]). This means that no model-independent measurement with such a network can possibly distinguish between the two, so it is enough for us to consider just one of them explicitly; we will refer to the scalar modes jointly by the subscript "s". (This degeneracy may not be present for detectors with different geometries [35, 36].)

The response of a given differential-arm detector to signals of certain linear polarization and direction of propagation can be written, in the local Lorentz frame of the detector itself, as [see e.g. Eqs. (13.98) in [34] with $\psi \to -\psi - \pi/2$, to account for the different wave-frame definition]:

$$F_+(\vartheta,\varphi,\psi) = -\frac{1}{2}\left(1+\cos^2\vartheta\right)\cos 2\varphi\cos 2\psi - \cos\vartheta\sin 2\varphi\sin 2\psi \,, \tag{18}$$

$$F_\times(\vartheta,\varphi,\psi) = \frac{1}{2}\left(1+\cos^2\vartheta\right)\cos 2\varphi\sin 2\psi - \cos\vartheta\sin 2\varphi\cos 2\psi \,, \tag{19}$$

$$F_{\rm x}(\vartheta,\varphi,\psi) = -\sin\vartheta\sin 2\varphi\cos\psi + \sin\vartheta\cos\vartheta\cos 2\varphi\sin\psi \,, \tag{20}$$

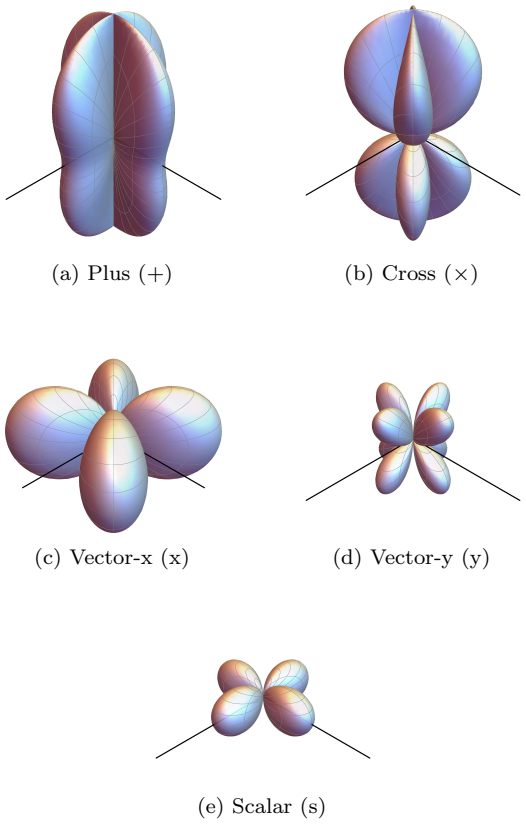

(a) Plus (+) (b) Cross (×) (c) Vector-x (x) (d) Vector-y (y) (e) Scalar (s)

FIG. 2. *Angular response of a quadrupolar detector to each GW polarization.* The radial distance represents the response of a single quadrupolar antenna to a unit-amplitude gravitational signal of a tensor (top), vector (middle), or scalar (bottom) polarization, i.e. $|F_A|$ for each polarization A as given by Eqs. (18–22) for $\psi = 0$. The polar and azimuthal coordinates correspond to the source location with respect to the detector, which is to be imagined as placed with its vertex at the center of each plot and arms along the x and y-axes. The response is plotted to scale, such that the black lines representing the detector arms have unit length in all plots. The response to breathing and longitudinal modes is identical, so we only display it once and label it "scalar". (Reproduced from [22].)

$$F_{\rm y}(\vartheta,\varphi,\psi) = \sin\vartheta\sin 2\varphi\sin\psi + \sin\vartheta\cos\vartheta\cos 2\varphi\cos\psi\ , \tag{21}$$

$$F_{\rm b/l}(\vartheta,\varphi,\psi) = \mp\frac{1}{2}\sin^2\vartheta\cos 2\varphi\ , \tag{22}$$

where ϑ and φ are the polar an azimuthal coordinates of the source with respect to the antenna at any given time (with detector arms along the x and y-axes). The tensor, vector and scalar nature of the different polarizations is evident in this form, given how each mode depends on ψ (i.e. how it transforms under rotations around the direction of propagation).

Equations (18)–(22) are represented in Fig. 2 by a spherical polar plot in which the radial coordinate corresponds to the sensitivity given by the magnitude $|F_A|$, shown for $\psi = 0$. The angular response functions have quadrupolar symmetry around the detector's zenith, regardless of the helicitiy of the polarization itself. This figure also makes it clear that differential-arm detectors will generally be more sensitive to some polarizations than others, although this will vary with the sky location of the source. For example, for all but a few sky locations, quadrupolar antennas will respond significantly less to a breathing signal than a plus or cross signal.

Fig. 2 shows the response of a single differential-arm detector to waves coming from different directions in the local frame of the instrument. However, we are usually interested in the sensitivity of a *network* of detectors, and its ability to distinguish the different polarizations. To visualize this, define the effective response to each of the helicities, for a given source sky-location (α, δ) and detector I:

$$|F^I_{\rm t}(\alpha,\delta)| \equiv \sqrt{F^I_+(\alpha,\delta)^2 + F^I_\times(\alpha,\delta)^2}\,, \tag{23}$$

$$|F^I_{\rm v}(\alpha,\delta)| \equiv \sqrt{F^I_{\rm x}(\alpha,\delta)^2 + F^I_{\rm y}(\alpha,\delta)^2}\,, \tag{24}$$

$$|F^I_{\rm s}(\alpha,\delta)| \equiv \sqrt{F^I_{\rm b}(\alpha,\delta)^2 + F^I_{\rm l}(\alpha,\delta)^2} = \sqrt{2}\,|F^I_{\rm b}(\alpha,\delta)|\,, \tag{25}$$

for tensor, vector and scalar waves respectively. (Here, since we are not dealing with any specific source, we *define* our polarization frame letting $\psi = 0$.) For a network of N detectors, we may then construct an effective response vector for each of the polarization sets above,

$$\vec{F}_H(\alpha,\delta) \equiv \left(|F^1_H(\alpha,\delta)|,\ldots,|F^N_H(\alpha,\delta)|\right), \tag{26}$$

for $H \in \{\rm t, v, s\}$. Finally, we may compare the overall sensitivity of the network to different polarizations by defining the *overlap*, as a normalized inner product between two of these vectors.

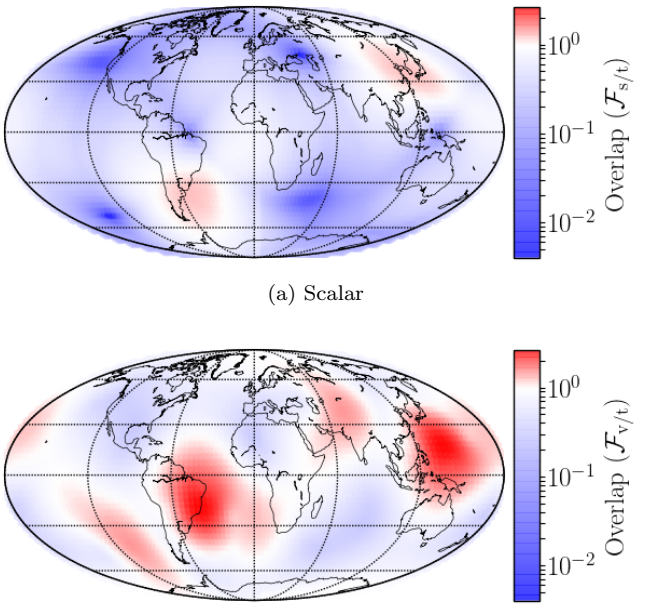

(a) Scalar

(b) Vector

FIG. 3. *Overlaps of LIGO-Virgo network effective antenna patterns.* The normalized inner-products of Eq. (27) for the three-instrument network. The top plot compares scalar to tensor ($\mathcal{F}_{\rm s/t}$), and the bottom one compares vector to tensor ($\mathcal{F}_{\rm v/t}$). Blue (red) marks regions for which the effective nontentor response is greater (less) than tensor. A map of Earth is overlaid for reference.

For instance, to compare the effective scalar or vector network sensitivity to the tensor one, we may look at the overlap factor:

$$\mathcal{F}_{H/\rm t}(\alpha,\delta) = \frac{\vec{F}_H(\alpha,\delta)\cdot\vec{F}_{\rm t}(\alpha,\delta)}{\vec{F}_{\rm t}(\alpha,\delta)\cdot\vec{F}_{\rm t}(\alpha,\delta)}, \tag{27}$$

which will take values greater (less) than unity if the response to polarizations H is better (worse) than to tensor, with $\mathcal{F}_{\rm t/t}(\alpha,\delta) = 1$ by construction. The scalar and vector overlaps with tensor are displayed for the LIGO-Virgo network in the skymap of Fig. 3, over a map of Earth for reference. Colored regions roughly correspond to areas in the sky for which the tensor and nontensor responses of the network are highly distinguishable. The patterns are anchored to angular locations with respect to Earth (not the fixed stars), and is determined by the specific location and orientation of the three detectors.

Averaged over all sky locations, the response of the network is worse for scalar signals than tensor ones, which is apparent from the top skymap in Fig. 3 and the distribution in Fig. 4. This is expected given that each interferometer is individually less sensitive to scalar waves, as seen in Fig. 2. On average, there is no significant difference between vector and tensor responses.

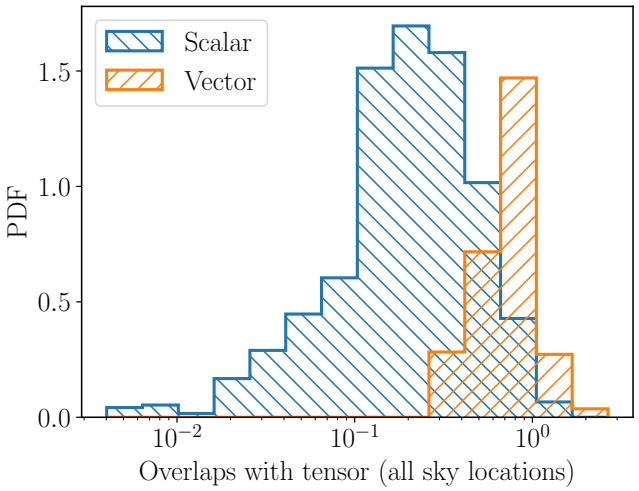

FIG. 4. *Overlaps of LIGO-Virgo network effective antenna patterns.* The normalized inner-products of Eq. (27) for the three-instrument network. The top plot compares scalar to tensor ($\mathcal{F}_{\rm s/t}$), and the bottom one compares vector to tensor ($\mathcal{F}_{\rm v/t}$). Blue (red) marks regions for which the effective nontentor response is greater (less) than tensor. A map of Earth is overlaid for reference.

III. METHOD

Ideally, we would like to unequivocally measure the polarizations of the GW that produced a given transient strain signal in our detector network. Formally, this would mean finding which of the seven possible Bayesian hypotheses the data favor: pure tensor ($\mathcal{H}_{\rm t}$), pure vector ($\mathcal{H}_{\rm v}$), pure scalar ($\mathcal{H}_{\rm s}$), scalar-tensor ($\mathcal{H}_{\rm st}$), vector-tensor ($\mathcal{H}_{\rm tv}$), scalar-vector ($\mathcal{H}_{\rm sv}$), or scalar-vector-tensor ($\mathcal{H}_{\rm stv}$). A comprehensive Bayesian treatment of this polarization model-selection problem was presented in [22] for the case of continuous signals from known pulsars, later applied to stochastic GW backgrounds in [23], and could be easily by adapted to the case of transient signals considered here.

Yet, a simple counting argument is enough to show that three detectors are not sufficient to break *all* degeneracies between the five distinguishable GW polarizations using transient signals [6, 8]. Therefore, with the current LIGO-Virgo network, we expect the results of an all-encompassing model-selection analysis, as discussed above, to be inconclusive or dominated by priors. Nevertheless, we may still attempt to distinguish between *some* of the possible hypotheses.

As mentioned in the introduction, *all LIGO-only observations so far are consistent with the extreme scenario of GWs being composed of purely vector or purely scalar polarizations.* Therefore, here we will focus on the problem of directly distinguishing between these theoretically far-fetched, yet phenomenologically valid, possibilities. That is, we will study our ability to choose between $\mathcal{H}_{\rm s}$ vs $\mathcal{H}_{\rm t}$, and between $\mathcal{H}_{\rm v}$ vs $\mathcal{H}_{\rm t}$. Importantly, this is qualitatively distinct from the more standard question about the presence of small nontensorial components in addition to the tensor wave predicted by GR. Although perhaps not as interesting as these "mixed" polarization studies (which, as explained above, will not fully succeed with current detectors), the problem of distinguishing between the "pure" polarization cases is well-defined and experimentally valuable.

We would like to ask the question: *is it geometrically possible that a given strain signal observed in the LIGO-Virgo network was produced by a GW with polarization other than GR's tensor + and ×?* The only way for us to answer this question is to probe the antenna patterns of our instruments, Eq. (11), which are a direct manifestation of local geometry only (polarizations and detector geometry), independent of source or the details of the underlying theory (see Sec. II B). We may thus exploit the difference in the response of the network to the different polarizations (Fig. 3).

One way to extract polarization information using the antenna patterns would be to construct linear combinations of the detector outputs that are guaranteed to contain no tensorial signal [8]. If coherent power (as seen by, e.g. a wavelet analysis) remains in such a *null-stream*, then that signal could not have been produced by a tensor (GR) wave. This approach has the strong advantage that it requires no knowledge of the spectral features of the signal whatsoever. However, to construct null-streams one needs to very accurately know the location of the source *a priori*, which is never the case without an electromagnetic counterpart (or more detectors).

Alternatively, one could carry out a morphology-independent sine-Gaussian analysis (e.g. using `BayesWave` [37, 38]) to reconstruct the best-fit unmodeled waveform from the data, and use that to extract information about times of arrival, phase offsets and relative amplitudes at different detectors. One could then just replace the tensor antenna patterns used in the signal reconstruction by their scalar or vector counterparts, and see how well each case fits the data (as measured by a Bayes factor). In such test, *no polarization information is extracted from the phase evolution.* In particular, the waveform reconstruction is only used to infer the source location from the time lag between detectors, and the best-fitting combination of antenna patterns from the amplitudes and phases at peak energy. (See pedagogical example in Sec. III A below.) An analysis like this was implemented for scalar modes and applied to the GW150914 signal, yielding no conclusive results as mentioned above [5].

However, all signals observed by LIGO so far are exceptionally well described by GR CBC waveforms [2–5]. This match is established on a case-by-case basis through comparisons between the GR templates and morphology independent burst reconstructions of the signal in the data, and is largely independent of the polarization. In fact, for any of these confident detections, the waveform reconstructed from burst analyses is effectively identical to a GR template. As emphasized above, in the pure-

polarization test ($\mathcal{H}_{\rm s}$ vs $\mathcal{H}_{\rm t}$, or $\mathcal{H}_{\rm v}$ vs $\mathcal{H}_{\rm t}$) all that matters is that most of the signal power is captured by the template, regardless of small potential mismatches in the phasing. Therefore, we may carry out the same study proposed in the previous paragraph using GR waveforms to fit the data, while replacing the tensor antenna patterns with those of different polarizations.

In other words, when the signal is clearly well-captured by a GR template, we may use that directly to extract polarization information from the antenna patterns in a model independent way, without implicitly assuming that the GW that caused it was tensor polarized as GR predicts. The waveform reconstruction will be dominated by the measurement at the most sensitive detector, while the amplitude information is encoded in the relations between measurements by different detectors.

Whether we use GR templates or a collection of sine-Gaussians to reconstruct the waveform, the effect of changing the antenna patterns will always result in different inferred sky location and orientation for the source. Yet, not all antenna patterns will be equally consistent with the observed relative amplitudes, phase offsets and delays between the signals in our three detectors—this will result in a poorer signal likelihood, and hence odds favoring tensor vs nontensor. Precisely because the waveform used to capture the signal is the same, we know that any difference between the tensor and nontensor results *must* come from the antenna patterns (polarizations).

This approach does not extract any information from the specific phase evolution of the signal, and is insensitive to small changes in the waveform. Therefore, using a GR template to measure the signal power is justified, and does not imply a contradiction when testing for nontensorial polarizations. For the purpose of this study, the CBC signal is just probing the impulse response function of our network, and the same results would be obtained if the waveform was just a Delta function rather than a chirp.

A. Toy example

For concreteness, consider the example of an elliptically-polarized, two-component GW (e.g. two tensor modes, or two vector modes) with waveform roughly described by a simple sine-Gaussian wavepacket, with some characteristic frequency Ω and relaxation time τ. Letting t be the time measured at Earth's center, then the strain measured by a given detector I will be:

$$h_I(t) = \Re\left[A\left(F_1^I + i\epsilon F_2^I\right) e^{i\Omega(t-t_0-\delta t_I)}\right] e^{-(t-t_0-\delta t_I)^2/\tau^2}, \tag{28}$$

where F_1^I and F_2^I are the responses of detector I to the two polarizations, $A \equiv |A| e^{i\phi_0}$ is a complex-valued amplitude, ϵ is an ellipticity parameter controlling the relative amounts of each polarization, and $\Re$ denotes the real part. Also, t_0 marks the time of arrival at Earth's center, which is delayed with respect to each interferometer by

$$\delta t_I = \hat{\mathbf{n}} \cdot \mathbf{x}_I / c\,, \tag{29}$$

where $\hat{\mathbf{n}}$ is a unit vector from Earth to the source, and $\mathbf{x}_I$ joins Earth's center to the detector (with magnitude equal to Earth's radius). Here we are assuming that the GW travels at the speed of light, c.

The signal of Eq. (28) may be written more simply as

$$h_I(t) = \mathcal{A}_I \cos[\Omega(t-\Delta t_I) + \Phi_I]\, e^{-(t-\Delta t_I)^2/\tau^2}\,, \tag{30}$$

after defining the three main observables at each detector:

$$\mathcal{A}_I \equiv |A|\left|F_1^I + i\epsilon F_2^I\right|\,, \tag{31}$$

$$\Phi_I \equiv \phi_0 + \arctan(\epsilon F_2^I / F_1^I)\,, \tag{32}$$

$$\Delta t_I \equiv t_0 + \delta t_I \tag{33}$$

From the output of three detectors (H, L, V), we may implement a simple inference analysis to extract these three numbers for the signal as seen by each instrument. The times at peak amplitude provide the three Δt_I's, while measurements of the phase and amplitude at peak itself give the Φ's and $\mathcal{A}_I$'s respectively. As always, recovery of all these parameters will be negatively affected by instrumental noise.

The three timing measurements alone suffice to recover the sky location of the source, $\hat{\mathbf{n}}$. With this knowledge, it is then possible to compute the values of all the corresponding antenna response functions, and thus obtain predictions for the $(F_1^I + i\epsilon F_2^I)$ factors for any given ellipticity. Ratios of amplitudes and phase differences between detectors may then be used to infer measured values for these quantities, and then find the best fitting polarization model. This may be achieved, for instance, via a maximum-likelihood analysis, effectively minimizing the distance between vectors like those of Eq. (26) and a similar one inferred from the data. (Note $|A|$, ϕ_0, and ϵ are nuisance parameters, and can be marginalized over.)

Although for this example we used a simple sine-Gaussian wavepacket to measure the signal, at no point we made use of the specific details of this phase evolution. The only requirement is that the GW have a well-defined peak, in order to extract meaningful information about how the relative timing, phase and amplitude of this peak as seen by different detectors. In particular, this analysis would work precisely the same way if CBC-like chirp waveform was used, as long as most of the power in the actual signal is indeed captured by such a template.

This toy analysis makes the dependence on A_I, Φ_I, Δt_I explicit. In reality, when studying actual data, one would ideally implement a full Bayesian analysis, marginalizing over all parameters to compute evidences for the different polarization hypotheses ($\mathcal{H}_{\rm t}$, $\mathcal{H}_{\rm v}$, $\mathcal{H}_{\rm s}$), and to produce the Bayes factors (likelihood ratios) of interest. The polarization information extracted by this more rigorous analysis would still, nonetheless, effectively come from the values of A_I, Φ_I, Δt_I. As emphasized before, this is the case whether one uses GR templates or a collection of sine-Gaussians to capture the signal power.

IV. CONCLUSION

By extracting polarization information from the antenna patterns we may directly probe the geometry of the GW metric perturbation (i.e. the directions along which space is stretched and squeezed by the passing wave) from its projection onto our detector network. With transient signals, instruments at five or more different orientations would be needed to break all degeneracies between the five independent (as seen by differential-arm detectors) polarizations allowed by generic metric theories of gravity. However, we may already distinguish between some of the possibilities using the current LIGO-Virgo network. How well we can do this will depend on the specific properties of each transient event (mainly, sky location).

The kind of geometric observational statement discussed in this note is independent of any theory or source model, and is only possible with the addition of Virgo to the network. Although here we focused on the problem of distinguishing between "pure" polarization states (tensor, vector or scalar), the case of "mixed" polarizations will be addressed in future work. More details and a demonstration of the analysis proposed here on simulated signals will be provided soon in an expanded version of this document.

ACKNOWLEDGMENTS

LIGO was constructed by the California Institute of Technology and Massachusetts Institute of Technology with funding from the National Science Foundation and operates under cooperative agreement PHY-0757058. This paper carries LIGO Document Number LIGO-P1700276.

[1] B. P. Abbott et al., (The LIGO Scientific Collaboration, and The Virgo Collaboration), Phys. Rev. Lett. **116**, 061102 (2016).
[2] B. P. Abbott et al., (The LIGO Scientific Collaboration, and The Virgo Collaboration), Phys. Rev. Lett. **116**, 241103 (2016).
[3] (The LIGO Scientific Collaboration and The Virgo Collaboration), Phys. Rev. X **6**, 041015 (2016), arXiv:1606.04856.
[4] B. P. Abbott, (The LIGO Scientific Collaboration, and The Virgo Collaboration), Phys. Rev. Lett. **118**, 221101 (2017), arXiv:1706.01812.
[5] B. P. Abbott et al., (The LIGO Scientific Collaboration, and The Virgo Collaboration), Phys. Rev. Lett. **116**, 221101 (2016), arXiv:1602.03841.
[6] C. M. Will, *Theory and experiment in gravitational physics*, revised ed ed. (Cambridge University Press, Cambridge, 1993).
[7] C. M. Will, Living Rev. Relativ. **17** (2014), 10.12942/lrr-2014-4.
[8] K. Chatziioannou, N. N. Yunes, and N. Cornish, Phys. Rev. D **86**, 022004 (2012), arXiv:1204.2585.
[9] J. M. Weisberg, D. J. Nice, and J. H. Taylor, Astrophys. J. **722**, 1030 (2010), arXiv:1011.0718.
[10] P. C. C. Freire, N. Wex, G. Esposito-Farèse, J. P. W. Verbiest, M. Bailes, B. A. Jacoby, M. Kramer, I. H. Stairs, J. Antoniadis, and G. H. Janssen, Mon. Not. R. Astron. Soc. **423**, 3328 (2012).
[11] I. H. Stairs, Living Rev. Relativ. **6**, 5 (2003).
[12] N. Wex, "Testing Relativistic Gravity with Radio Pulsars," (2014), arXiv:1402.5594.
[13] Z. Berezhiani, D. Comelli, F. Nesti, and L. Pilo, Phys. Rev. Lett. **99**, 131101 (2007), arXiv:0703264 [hep-th].
[14] S. Hassan, A. Schmidt-May, and M. von Strauss, J. High Energy Phys. **2013**, 86 (2013), arXiv:1208.1515.
[15] K. Max, M. Platscher, and J. Smirnov, Phys. Rev. Lett. **119**, 111101 (2017), arXiv:1703.07785.
[16] P. Brax, A.-C. Davis, and J. Noller, Phys. Rev. D **96**, 023518 (2017), arXiv:1703.08016.
[17] B. Pontecorvo, Sov. Phys. JETP **6**, 429 (1957).
[18] B. Pontecorvo, Sov. Phys. JETP **26**, 984 (1968).
[19] S. Alexander and N. Yunes, Phys. Rep. **480**, 1 (2009), arXiv:0907.2562.
[20] D. M. Eardley, D. L. Lee, A. P. Lightman, R. V. Wagoner, and C. M. Will, Phys. Rev. Lett. **30**, 884 (1973).
[21] D. Eardley, D. Lee, and A. Lightman, Phys. Rev. D **8**, 3308 (1973).
[22] M. Isi, M. Pitkin, and A. J. Weinstein, Phys. Rev. D **96**, 042001 (2017), arXiv:1703.07530.
[23] T. Callister, A. S. Biscoveanu, N. Christensen, M. Isi, A. Matas, O. Minazzoli, T. Regimbau, M. Sakellariadou, J. Tasson, and E. Thrane, "Tests of General Relativity with the Stochastic Gravitational-Wave Background," (2017), arXiv:1704.08373.
[24] K. S. Thorne, D. L. Lee, and A. P. Lightman, Phys. Rev. D **7**, 3563 (1973).
[25] C. Brans and R. H. Dicke, Phys. Rev. **124**, 925 (1961).
[26] D. Andriot and G. L. Gómez, J. Cosmol. Astropart. Phys. **2017**, 048 (2017), arXiv:1704.07392.
[27] A. P. Lightman and D. L. Lee, Phys. Rev. D **8**, 3293 (1973).
[28] N. Rosen, Ann. Phys. (N. Y). **84**, 455 (1974).
[29] C. de Rham, Living Rev. Relativ. **17** (2014), 10.12942/lrr-2014-7, arXiv:1401.4173.
[30] C. Mead, "Gravitational Waves in G4v," (2015), arXiv:1503.04866.
[31] A. Nishizawa, A. Taruya, K. Hayama, S. Kawamura, and M.-a. Sakagami, Phys. Rev. D **79**, 082002 (2009), arXiv:0903.0528.
[32] A. Błaut, Phys. Rev. D **85**, 043005 (2012).
[33] M. Isi, A. J. Weinstein, C. Mead, and M. Pitkin, Phys. Rev. D **91**, 082002 (2015).
[34] E. Poisson and C. M. Will, *Gravity: Newtonian, Post-Newtonian, Relativistic* (Cambridge University Press, Cambridge, 2014).
[35] K. J. Lee, F. A. Jenet, and R. H. Price, Astrophys. J. **685**, 1304 (2008).
[36] S. J. Chamberlin and X. Siemens, Phys. Rev. D **85**, 082001

(2012), arXiv:1111.5661.
[37] N. J. Cornish and T. B. Littenberg, Class. Quantum Gravity **32**, 135012 (2014), arXiv:1410.3835.
[38] T. B. Littenberg, J. B. Kanner, N. J. Cornish, and M. Millhouse, Phys. Rev. D **94**, 044050 (2016), arXiv:1511.08752.